H_2S Stability of Metal-Organic Frameworks: A computational assessment

Pengbo Lyu and Guillaume Maurin*

ICGM, Univ. Montpellier, CNRS, ENSCM, Montpellier, France

Abstract

The H_2S stability of a range of MOFs was systematically assessed by first-principle calculations. The most likely degradation mechanism was first determined and we identified the rate constant of the degradation reaction as a reliable descriptor for characterizing the H_2S stability of MOFs. A qualitative H_2S stability ranking was thus established for the list of investigated materials. Elemental structure-stability relationships were further envisaged considering several variables including the nature of the linkers and their grafted functional groups, the pore size, the nature of metal sites and the presence/nature of coordinatively unsaturated sites. This knowledge enabled the anticipation of the H_2S stability of one prototypical MOF, e.g. MIL-91(Ti), which has been previously proposed as a good candidate for CO_2 capture. This computational strategy enables an accurate and easy handling assessment of the H_2S stability of MOFs and offers a solid alternative to experimental characterizations that require the manipulation of a highly toxic and corrosive molecule.

Keywords: Metal-organic frameworks, Hydrogen disulfide, Prediction of stability, Understanding of Degradation Mechanism, Density Functional Theory.

1. Introduction

Metal-Organic Frameworks (MOFs), a class of highly crystalline and tunable porous materials, have been envisaged over the past several years for a myriad of applications in the fields of catalysis,[1-3] gas adsorption/separation,[4-7] biomedicine[8-9] and sensing[10-11] among others.[12-14] While their performances sometimes outperform the well-established porous media such as zeolites, silica and carbons, this family of hybrid materials is still not yet widely applied to industry since most of the studies rarely report their chemical stability under working conditions. Typically, the performances of MOFs are promising to solve challenges in critical industrial applications such as CO_2 capture,[6, 15-19] flue gas scrubbing,[20-23] natural gas (NG) and refinery-off gases (ROG) upgrading.[24-27] This critically calls for a systematic exploration of the stability of the best MOFs upon exposure to impurities present in the associated flue gas streams[28-30] such as H_2O, H_2S, SO_x, and NO_x among others to meet the industry's expectation in this field.[31] While the stability of MOFs upon water adsorption is routinely assessed from both experimental[32-37] and modeling[38-42] standpoints, this is far to be the case under harsh conditions as for instance in the presence of acidic and basic species.[43-44] Only a small fraction of MOFs promising for CO_2 capture, natural gas or bio-gas purification has been tested in terms of stability upon exposure to NO_x, SO_x, H_2S and NH_3[44-48]. Specifically, related to H_2S, while a series of MOFs have been envisaged for the capture of this highly toxic molecule, [20, 24, 45, 49-56] such as MIL-53(Al, Cr) and MIL-47(V),[50-51] **soc**-MOF,[24] kag-MOF-1,[20] MIL-125(Ti),[49] UiO-66,[52] Mg-CUK-1,[53] MIL-53(Al)-FA,[54] MFM-300(Sc)[45] and MIL-53(Al)-TDC,[55] the H_2S stability of only a very few promising MOFs for the applications mentioned above, e.g. KAUST-7,[56] KAUST-8,[56] kag-MOF-1,[20] **soc**-MOF[24], MIL-125(Ti)[49] and MOF-74(Ni),[57] has been verified. Beyond this observation, to the best of our knowledge no systematic exploration of the H_2S

stability of MOFs has been reported to date and understanding of the H_2S degradation mechanism is still far from clear. Indeed, while standard experimental techniques such as X-ray diffraction and Thermogravimetric analysis, [52, 58-62] have been used to characterize the stability of MOFs after exposure to H_2S, only a few *in situ* FT-IR study has been conducted to characterize the adsorption modes of H_2S in MOFs,[49-51, 53] however without paying attention on the H_2S degradation mechanism. From a computational standpoint, while the H_2S physisorption mechanism has been elucidated for a range of MOFs using force field based Monte Carlo (MC) simulations and Density Functional Theory (DFT) calculations,[24-25, 49, 51, 53, 55], none of these studies have addressed the question of H_2S stability/degradation.

Herein, the driving-step of the H_2S-induced MOF degradation reaction was explored systematically using periodic DFT calculations applied to a series of MOFs. To that purpose, we first evaluated different plausible degradation mechanisms with MIL-53(Al)-BDC[30] taken as our reference MOF material since it was already proved experimentally to be stable upon exposure to H_2S. This preliminary stage enabled us to identify the most probable degradation mechanism and to propose the rate constant of the degradation reaction as a reliable descriptor for characterizing the H_2S stability of MOFs. We further explored a range of MOFs with the objective to evaluate how the stability of this family of materials is affected by the nature of the linkers, with the consideration of several derivatives of MIL-53[54-55] and CAU-10;[63-65] the nature of the functional groups grafted to organic linkers, with the use of functionalized MIL-53(Al)s,[66-67] the pore size with the comparison between the large-pore and narrow-pore forms of MIL-53(Al)-BDC-NH_2,[67] the metal substitution with the cases of CAU-10(Al)[68] and MIL-160(Al)[69] and their Ti-analogues and the presence/nature of coordinatively unsaturated site (CUS) with the consideration of MOF-74 (Ni)[57] and MOF-74(Zn).[52, 57] This systematic exploration led to a

qualitative H_2S stability ranking of all these MOFs based on the evaluation of their associated rate constants for the corresponding first-step degradation reaction. This allowed to reveal elemental structure-stability relationship that was further transferred to anticipate the H_2S stability of the MOF MIL-91(Ti) as a show-case since this material has been proposed as a good candidate for the selective capture of CO_2 under flue gas conditions[70] while its H_2S stability was still unknown. We believe this computational approach allows an accurate and easy handling assessment of the H_2S stability of MOFs without the need to perform fastidious experiments due to the high toxicity and corrosive character of H_2S.

2. Computational methods

The unit cells of all empty MOFs were first geometry optimized at the DFT level starting with their known crystal structures. Note that for all structures showing lattice parameters below 12 Å, super-cells associated with a doubled cell parameter along the corresponding direction were constructed. These calculations used the projector augmented wave (PAW)[71] formalism within the generalized gradient approximation (GGA) method with Perdew-Burke-Ernzerhof (PBE) exchange-correlation functional as implemented in Vienna Ab Initio Simulation Package (VASP).[72-74] The DFT-D3 method[75] was employed to include the dispersion correction. A cut-off energy of 900 eV for the plane-wave basis set was considered to ensure convergence with the following criteria of 0.01 eV/Å and 10^{-5} eV for the forces and energy respectively. The Brillouin zone was sampled at gamma point. Note that for Ni- and Ti-containing MOFs, spin-polarization was considered together with DFT+U approach[76] to accurately describe the 3d states, where U_{eff} was selected to be 6.4 eV and 3.0 eV for Ni[77] and Ti[78] respectively. In addition, unlike Ti-MOFs which have zero magnetic moment, we found for MOF-74(Ni) that ferromagnetic (FM) intra-chain coupling is slightly more stable than the anti-ferromagnetic (AFM) one by 0.06 eV.

Therefore, the FM configuration for MOF-74(Ni) was selected for geometry optimization and subsequent calculations described below. Regarding the functionalized MIL-53(Al)-BDC, we considered the narrow pore (np) structure of MIL-53(Al)-BDC-NH_2 as well as its large pore (lp) form known to exist in the presence of guest molecules[67] while MIL-53(Al)-BDC-NO_2 was treated solely in its previous reported lp form.[66] The DFT-optimized lattice parameters of all empty MOFs are summarized in Table S1 along with the corresponding structures represented in Figures S1-S6. Starting with these DFT-optimized structures, 1 H_2S molecule was introduced per unit cell and the resulting guest-loaded configurations (labeled IS for Initial States) were further DFT-geometry optimized using the same settings mentioned above, their lattice parameters being maintained fixed. As a further stage, the H_2S degradation mechanism was explored, the transition states (TS) and the products (called final states (FS)) being identified using the climbing image nudged elastic band method (CI-NEB)[79] as implemented in the Transition State Tools for VASP (VTST) module.[80] Frequency calculations were performed for all minima (IS and FS) and transition state (TS) structures to ensure no imaginary frequency for both IS and FS and only 1 imaginary frequency for TS. Only the positions of the atoms involved in the first-step degradation reaction were relaxed during frequency calculations.

The potential energy (E) profile was then constructed by considering the optimized MOF unit cell and H_2S in the gas phase as zero-point potential energy. The reaction energy (ΔE) and its associated energy barrier ($\Delta E^{\ddagger}$) at 0 K were calculated using equations (1) and (2):

$$\Delta E = E(FS) - E(IS) \qquad (1)$$

$$\Delta E^{\ddagger} = E(TS) - E(IS) \qquad (2)$$

where E(X=IS, TS, FS) is the relative energy of the corresponding X configurations.

The rate constant (k) of the first-step H_2S degradation reaction was further considered as a more reliable descriptor than $\Delta E^{\ddagger}$ to quantitatively assess the stability of MOFs against H_2S at room temperature (298 K). Indeed, k explicitly reflects the chemical equilibrium between the three configurations (IS, TS and FS), rather than simply comparing the reaction energy barrier, $\Delta E^{\ddagger}$, which is insufficient to assess the difference between MOFs in terms of stability.

The k value was calculated using equation (3)

$$k = \exp\left(-\frac{\Delta G^{\ddagger}}{RT}\right) - \exp\left(-\frac{\Delta G^{\ddagger}_{r}}{RT}\right) \qquad (3)$$

where $\Delta G^{\ddagger}$ is the reaction free energy barrier; $\Delta G^{\ddagger}_{r}$ is the reversed reaction free energy barrier and T is the temperature (298 K). $\Delta G^{\ddagger}$ and $\Delta G^{\ddagger}_{r}$ were calculated as follows :

$$\Delta G^{\ddagger} = G(TS) - G(IS) \qquad (4)$$

$$\Delta G^{\ddagger}_{r} = G(TS) - G(FS) \qquad (5)$$

where G(X=IS, TS, FS) is the free energy of.the corresponding X configurations calculated as follows:[81]

$$G = E_0 + F_{vib}(v_i, T) \qquad (6)$$

where E_0 is the energy of the X configuration, and $F_{vib}(v_i, T)$ its corresponding Helmholtz vibrational energy defined as follows:

$$F_{vib}(v_i, T) = \frac{1}{2}\sum_i \left\{ h v_i + 2 k_b T \ln\left[1 - \exp\left(-\frac{h v_i}{k_b T}\right)\right] \right\} \qquad (7)$$

where h is Planck's constant, k_b is Boltzmann's constant, v_i is the harmonic vibrational frequency for relaxed atoms and T is set to 298 K.

According to the definition of k, a positive value indicates that the decomposition of the corresponding MOF is feasible upon exposure to H_2S, whereas a negative k value is a signature that the degradation is less probable. Since the first step of the degradation reaction is assumed to

be the predominant step in the reaction path, indeed more negative is k, more stable is the associated MOF against H_2S.

3. Results

3.1 Exploration of the plausible H_2S degradation mechanism and evaluation of the rate constant: MIL-53(Al)-BDC as a showcase

Referring to the mechanism proposed in the literature for the degradation of MOFs upon exposure to acid gas, e.g. SO_2,[82] we explored several possible H_2S first-step degradation reaction paths as shown in scheme 1.

(1) mechanism 1: one of the metal-oxygen bonds breaks and the created unsaturated μ-O atom is further coordinated by an hydrogen atom transferred from H_2S, while the remaining –SH group combines with the created coordinatively unsaturated Al site to form a metal-sulfur bond;

(2) mechanism 2: similarly to mechanism 1, an hydrogen atom of H_2S bounds the created unsaturated μ-O atom, however the –SH group coordinates to the carbon atom of the $–COO^-$ group;

(3) mechanism 3: the –SH group replaces the μ-OH hydroxyl function of the MOF to form two Al-S bonds, while the other hydrogen atom of H_2S combines with the released OH function to form a water molecule.

These three mechanisms were explored for MIL-53(Al)-BDC considered as a model MOF in our study and the different states along the reaction are illustrated in Figure 1. The most stable adsorption configurations of H_2S (IS) correspond to the scenario where its S-atom points towards the μ-OH group with a separating S(H_2S)-H(μ-OH) distance of 2.33 Å. For mechanism 1, one of the Al-O bonds breaks upon H_2S adsorption and the Al-S distance shortens along the reaction path as follows: 4.36 Å (IS)→ 2.62 Å (TS)→ 2.46 Å (FS) to finally form a bond, while the H-S

bond of H_2S dissociates (H-S distance : 1.35 Å (IS)→ 1.82 Å (TS)→3.29 Å (FS)). This mechanism is associated with a very high energy barrier ($\Delta E^{\ddagger}$) and a highly endothermic reaction energy (ΔE) of 169 kJ mol^{-1} and 115 kJ mol^{-1} respectively. For mechanism 2, the reaction proceeds via a significant reduction of the S-C distance between S(H_2S) and C(COO-) from 4.70 Å (IS) to 2.56 Å (TS) prior to form a S-C bond of 1.94 Å (FS) while one of the H-S bonds of H_2S breaks along the reaction path 1.35 Å (IS) → 2.00 Å (TS) → 2.64 Å (FS). This degradation mechanism is also highly endothermic (ΔE=117 kJ mol^{-1}) and the associated energy barrier ($\Delta E^{\ddagger}$ =146 kJ mol^{-1}) is as high as the value obtained for mechanism 1. Considering the fact that the protonation of the oxygen atom of the carboxylate group does not lead to an uncoordinated Al site, this mechanism was excluded since no further degradation of the framework can be expected. For mechanism 3, similar to mechanism 1, there is formation of an Al-S bond along the reaction path as seen by the evolution of the corresponding Al-S distance (4.36 Å (IS) → 2.30 Å (TS) → 2.38 Å (FS)). Although the resulting reaction energy ΔE (123 kJ mol^{-1}) is only slightly higher than the value obtained for mechanism 1 (115 kJ mol^{-1}), its energy barrier $\Delta E^{\ddagger}$ is much higher (256 *vs* 169 kJ mol^{-1}). This trend is explained by the fact that mechanism 3 proceeds via the breaking of 2 metal-oxygen bonds. Therefore this set of calculations demonstrates that mechanism 1, where only one of the metal-oxygen bonds breaks and one metal-sulfur bond forms, is the most likely first step of the MOF degradation upon exposure to H_2S. This mechanism 1 was thus systematically explored for the whole investigated MOFs. We assumed a similar first-step degradation reaction mechanism for all MOFs described above.

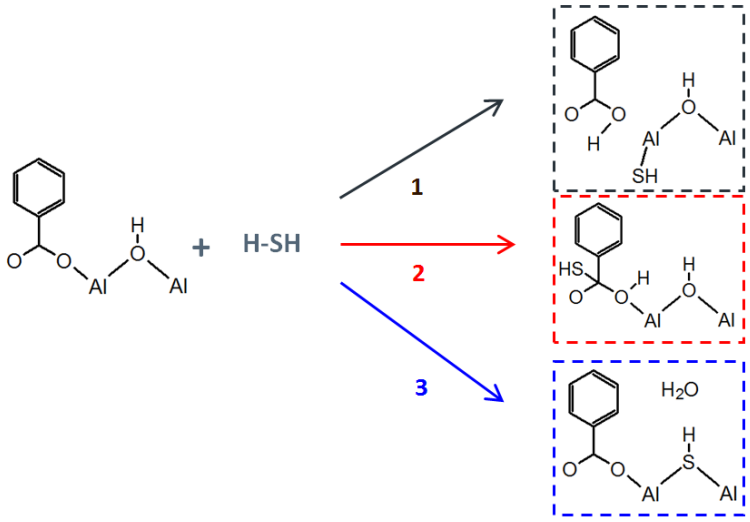

Scheme 1: The three different mechanisms of the first-step degradation reaction between H_2S and MOFs with MIL-53(Al)-BDC as a model system.

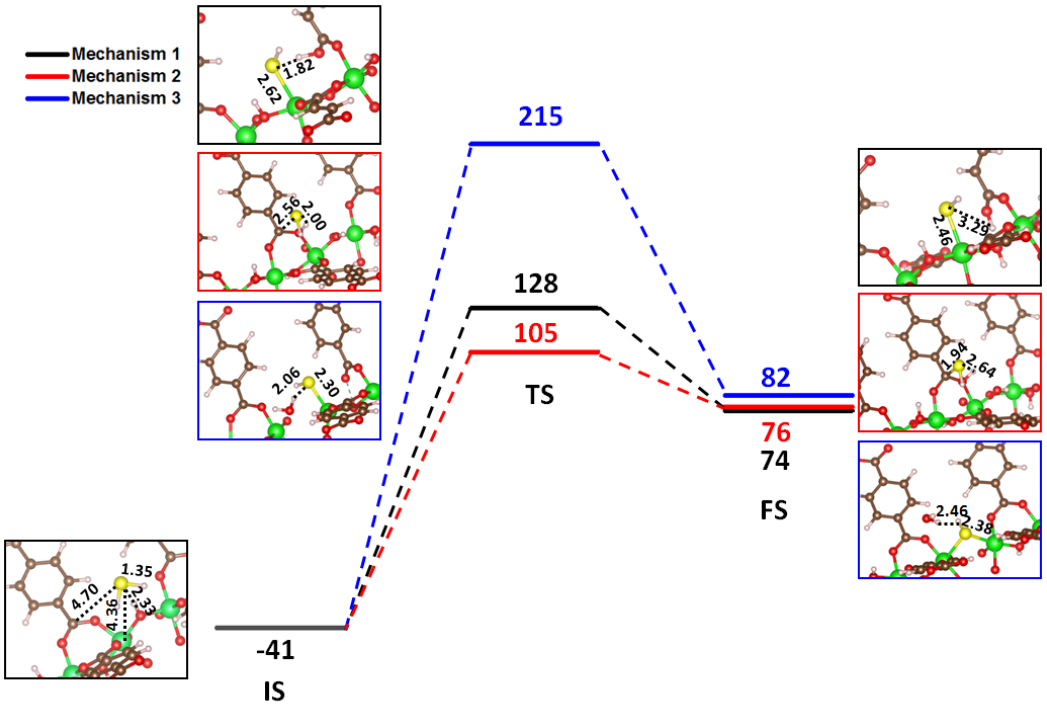

Figure 1: Potential energy profile for the three different H_2S degradation mechanisms explored in the case of MIL-53(Al)-BDC with the associated relative energies for the Initial States (IS), Transition States (TS) and Final States (FS). An illustration of the IS, TS and FS configurations is also provided. Color codes are carbon (brown), oxygen (red), sulfur (yellow), hydrogen (white) and aluminum (green). The corresponding energies and distances are reported in kJ mol^{-1} and Å respectively.

Furthermore, the calculated k value for the degradation mechanism 1 was found to be -4.9×10^{-9}. Indeed, since MIL-53(Al)-BDC was previously demonstrated to be stable against H_2S experimentally, this value was considered in the following sections as a reference to assess the stability of the series of MOFs. Indeed all MOFs associated with similar or even more negative k values will be considered as stable materials upon exposure to H_2S. Therefore, this descriptor was used to rank qualitatively the H_2S stability of all MOFs described above.

3.2 Impact of the nature of linkers on the H_2S stability of Al-MOFs

3.2.1. MIL-53(Al) frameworks

The first-step degradation reaction paths and the corresponding potential energy profiles for MIL-53(Al)-FA and MIL-53(Al)-TDC are compared with those for MIL-53(Al)-BDC in Figure 2. The most stable adsorption configurations of H_2S (IS) for both MIL-53(Al)-FA and MIL-53(Al)-TDC are similar to that observed for MIL-53(Al)-BDC with a predominant interaction between S(H_2S) and H(μ-OH). It is worth noting that the configurations of TS and FS along the reaction paths are also quite similar for the three different MOFs. The reaction energy barrier $\Delta E^{\ddagger}$ for MIL-53(Al)-FA (165 kJ mol^{-1}) is very close to that for MIL-53(Al)-BDC (169 kJ mol^{-1}), while the associated reaction energy ΔE is slightly lower (102 vs 115 kJ mol^{-1}). Interestingly, MIL-53(Al)-TDC shows a significanly lower $\Delta E^{\ddagger}$ (126 kJ mol^{-1}) but a similar ΔE (103 kJ mol^{-1}) as compared to the values found for the two other isoreticular forms.

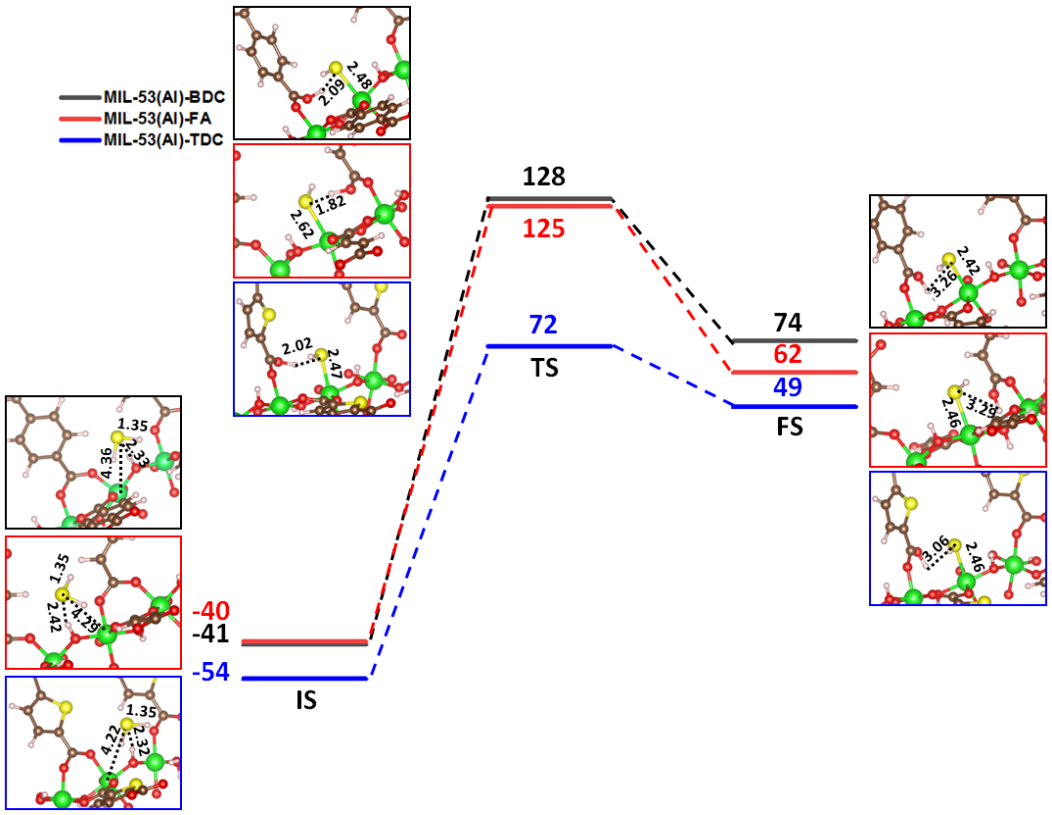

Figure 2: Potential energy profiles for the first-step H_2S degradation reaction by MIL-53(Al)-BDC (black line), -FA (red line) and -TDC (blue line). Color code is the same as in Figure 1. The corresponding energies and distances are reported in kJ mol^{-1} and Å respectively.

Although MIL-53(Al)-TDC shows the lowest $\Delta E^{\ddagger}$, it does not mean that it is the least stable one out of the three MOFs. Indeed, Table 1 which reports the reaction free energy barriers ($\Delta G^{\ddagger}$), the reversed reaction free energy barriers ($\Delta G^{\ddagger}_{r}$) and the rate constant (k) values for the 3 isoreticular MOFs at 298 K, shows that MIL-53(Al)-TDC is by far the most stable one, since its associated k value is much more negative (-1.1×10^{-3}) as compared to the values obtained for both MIL-53(Al)-BDC (-4.9×10^{-9}) and MIL-53(Al)-FA (-1.4×10^{-9}). These calculations predict the following sequence in terms of stability: MIL-53(Al)-TDC)>>MIL-53(Al)-BDC ~ MIL-53(Al)-FA since the two last MOFs show k values of similar magnitude. This trend is consistent with the very good H_2S adsorption/desorption cyclability of MIL-53(Al)-TDC previously

reported[55] as well as a similar stability of MIL-53(Al)-FA[54] and MIL-53(Al)-BDC.[30] The combination of a lower $\Delta E^{\ddagger}$ with a similar ΔE finally leads to a more negative k (and higher stability) for MIL-53(Al)-TDC. This observation confirms the reliability of the rate constant as a descriptor to assess the H_2S stability of MOFs.

Table 1: Reaction free energy (ΔG), reaction free energy barrier ($\Delta G^{\ddagger}$), reversed free energy barrier ($\Delta G^{\ddagger}_{r}$) and rate constants of the first-step H_2S degradation reaction (k) for all investigated MOFs. All the energies are reported at 298 K in kJ mol^{-1}.

	ΔG	$\Delta G^{\ddagger}$	$\Delta G^{\ddagger}_{r}$	K
MIL-53(Al)-BDC	133	180	47	-4.9×10^{-9}
MIL-53(Al)-FA	117	168	50	-1.4×10^{-9}
MIL-53(Al)-TDC	117	134	17	-1.1×10^{-3}
MIL-160(Al)-Furan	130	176	46	-9.0×10^{-9}
CAU-10(Al)-BDC	118	178	60	-3.3×10^{-11}
CAU-23(Al)-TDC	122	147	25	-4.0×10^{-5}
lp-MIL-53(Al)-BDC-NO_2	141	183	42	-4.3×10^{-8}
lp-MIL-53(Al)-BDC- NH_2	163	208	45	-1.5×10^{-8}
np-MIL-53(Al)-BDC-NH_2	168	206	38	-2.5×10^{-7}
CAU-10(Ti)-BDC	63	129	66	-2.8×10^{-12}
MIL-160(Ti)-Furan	74	122	48	-4.4×10^{-9}
MOF-74(Ni)	87	118	31	-5.5×10^{-6}
MOF-74(Zn)	13	75	61	-2.0×10^{-11}
MIL-91 (Ti)	145	163	18	-8.3×10^{-4}

3.2.2 CAU-10(Al)-BDC, MIL-160(Al)-Furan and CAU-23(Al)-TDC frameworks

In complement to 3.2.1, the H_2S stability of CAU-10(Al)-BDC, its furan derivative (MIL-160(Al)-Furan) and a similar structure integrating TDC linker (CAU-23(Al)-TDC) were explored.

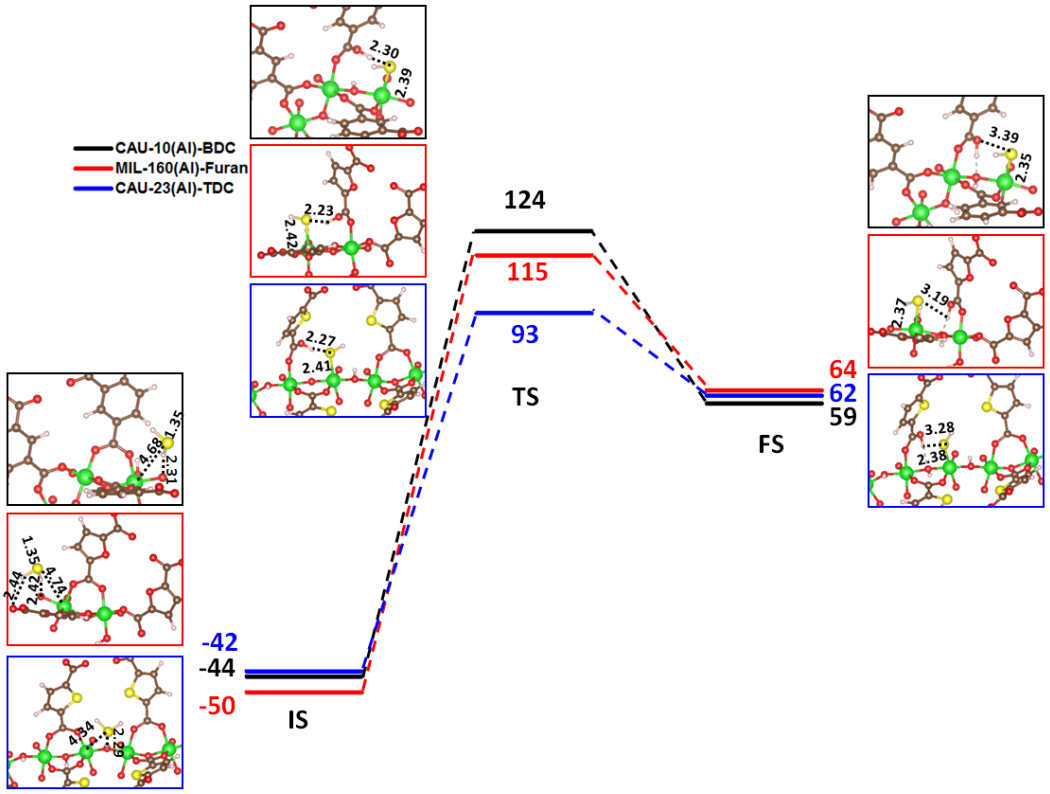

Figure 3: Potential energy profiles for first-step H_2S degradation reaction by CAU-10(Al)-BDC (red line), MIL-160(Al)-Furan (black line) and CAU-23(Al)-TDC (blue line). Color code is the same as in Figure 1. The corresponding energies and distances are reported in kJ mol^{-1} and Å respectively.

Compared to MIL-53 MOFs, while CAU-23(Al)-TDC shows the same adsorption mode with the interactions between S(H_2S) and H(μ-OH), CAU-10 derivatives (CAU-10(Al)-BDC and MIL-160(Al)-Furan) show different H_2S adsorption configurations because their μ-OH sites are not sterically accessible to guest. Indeed, H_2S interacts with the oxygen atom of the carboxylate groups. Figure 3 and Table 1 reveal that despite CAU-23(Al)-TDC shows the lowest energy barrier $\Delta E^{\ddagger}$, its associated k value is much more negative than for CAU-10(Al)-BDC. This trend which is the same than that observed between MIL-53(Al)-TDC and MIL-53(Al)-BDC, strongly suggests that the incorporation of TDC linker tends to reinforce the H_2S stability of the MOF architecture. MIL-160(Al)-Furan built with a heteroatom containing linker is expected to be also more stable than the CAU-10(Al)-BDC since its associated k value is more negative by two

orders of magnitude, leading to the following sequence in terms of stability: CAU-23(Al)-TDC>>MIL-160(Al)-Furan>CAU-10(Al)-BDC. Indeed, more generally, the inclusion of heteroatoms (sulfur and oxygen) in the linkers make MIL-53 and CAU-10 structures more stable. On the other hand, by comparing the scenarios for MIL-53(Al)-TDC/CAU-23(Al)-TDC and MIL-53(Al)-BDC/CAU-10(Al)-TDC, we found that the rate constants of MIL-53 frameworks are always slightly more negative than CAU-10/CAU-23 MOFs containing the same linker. This suggests that MIL-53(Al) is expected to be slightly more stable than CAU-10 (Al)/CAU-23(Al). This might be du to a slightly different vibrational contribution for MIL-53(Al) vs CAU-10 (Al)/CAU-23(Al) leading to a small variation of the free energies and k values.

3.3 Impact of the nature of the functional groups grafted to the organic linker on the H_2S stability of Al-MOFs

The stability of MIL-53(Al)-BDC was further compared with that of its functionalized derivatives with $–NO_2$ and $–NH_2$ groups considering in all cases a lp structure.

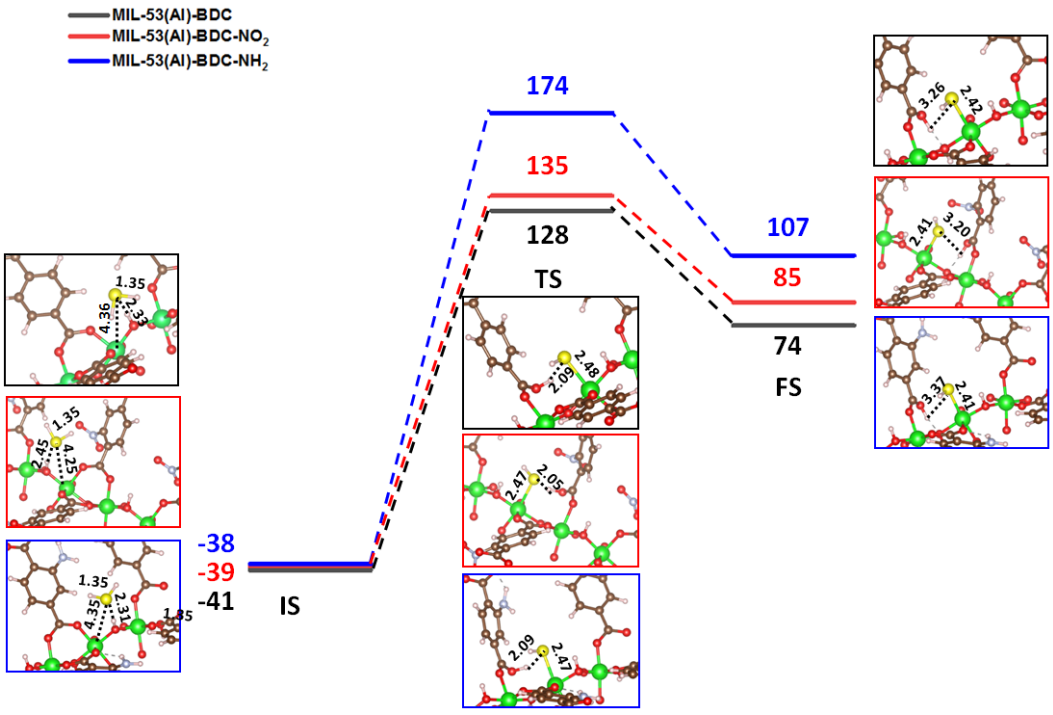

Figure 4: Potential energy profiles for first-step H_2S degradation reaction by MIL-53(Al)-BDC (black line), MIL-53(Al)-BDC-NO_2 (red line) and MIL-53(Al)-BDC-NH_2 (blue line). Color code is the same as in Figure 1 except nitrogen (light blue). The corresponding energies and distances are reported in kJ mol^{-1} and Å respectively.

Compared to the pristine MIL-53(Al)-BDC, the functionalization does not affect the predominant interactions between H_2S and μ-OH, as shown in Figure 4 since the separating distances between H_2S and $–NH_2$/$–NO_2$ groups are longer than 3 Å. The potential energy profiles shift upwards upon functionalization, while the structures of each state along the reaction paths remain similar, as shown in Figure 4. The higher energy barrier $\Delta E^{\ddagger}$ and reaction energy ΔE for MIL-53(Al)-NO_2 and MIL-53(Al)-BDC-NH_2 result from the introduction of relatively bulky functional groups which causes higher energy penalty for the H_2S-induced structural changes. As shown in Table 1, the rate constants k calculated for both functionalized forms are slightly more negative than the value obtained for MIL-53(Al)-BDC, suggesting the following stability sequence: MIL-53(Al)-BDC-NO_2~MIL-53(Al)-BDC-NH_2>MIL-53(Al)-BDC. Indeed this series of calculations predicts that the functionalization of the BDC linker, a strategy often employed to enhance the affinity of the MOF for a polar molecule,[67] does not play a detrimental role on the H_2S stability of the framework.

3.4 Impact of the pore size on the H_2S stability of Al-MOFs

MIL-53(Al)-BDC-NH_2 in both its lp and np forms was considered as a prototypical model to verify if the pore size can affect the MOF stability upon exposure to H_2S. The IS configuration for the np form corresponds to an interaction between S(H_2S) and the μ-OH group in a similar way than in the lp version. Figure 5 shows that the potential energy profiles are very similar in both cases while Table 1 evidences that the rate constant for np-NH_2-MIL-53(Al) is only slightly more negative than that for the lp structure. The relative energy of the FS configuration for the

np structure is slightly higher than that for the lp version, while the relative energies of the IS and TS configurations for lp and np structures are quite similar. This whole observation suggests that a higher degree of pore confinement is expected to induce only a tiny change of the stability of the MOF framework agains H_2S,.

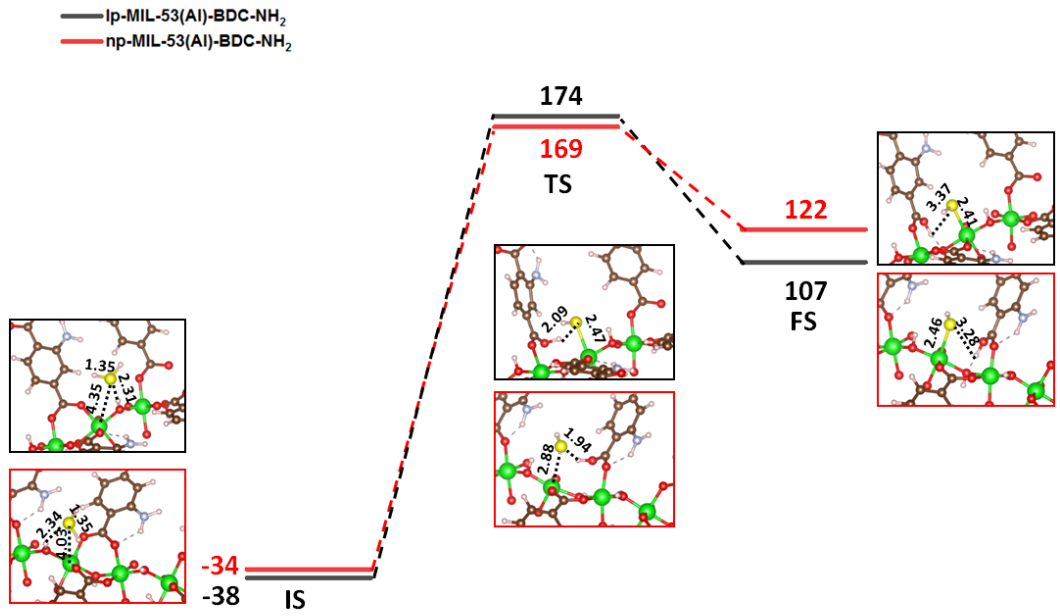

Figure 5: Potential energy profiles for first-step H_2S degradation reaction by lp-MIL-53(Al)-BDC-NH_2 (black line) and np- MIL-53(Al)-BDC-NH_2 (red line). Color code is the same as in Figure 4 except nitrogen (light blue). The corresponding energies and distances are reported in kJ mol^{-1} and Å respectively.

3.5 Impact of the substitution of Al^{3+} by Ti^{4+} metal sites on the H_2S stability of MOFs

As a typical illustration, the H_2S stability of CAU-10(Al)-BDC and MIL-160(Al)-Furan was compared with that of the hypothetical frameworks where Al^{3+} was substituted by Ti^{4+}, the hydroxyl μ-OH functions bridging the metal sites being replaced by μ-O oxo functions to keep the framework neutral. Figure 6 shows that the H_2S adsorption configurations (IS) for MIL-160(Ti)-Furan and CAU-10(Ti)-BDC correspond to an interaction between H(H_2S) and μ-O (see Figure 3).

The resulting potential energy profiles for the Ti-MOFs shift downwards and both the energy barriers and reaction energies are significantly lower as compared to their values for the aluminum analogues (see Figure 6 vs Figure 3). Nevertheless, the rate constants calculated for MIL-160(Ti)-Furan and CAU-10(Ti)-BDC (see Table 1) are only sligtly more negative than the values for their Al analogues, indicating that the substitution of Al^{3+} by Ti^{4+} in these MOFs which is expected to make them more hydrophobic will not deteriorate their stability against H_2S. Moreover MIL-160 remains more stable than CAU-10 whatever the nature of the metal sites.

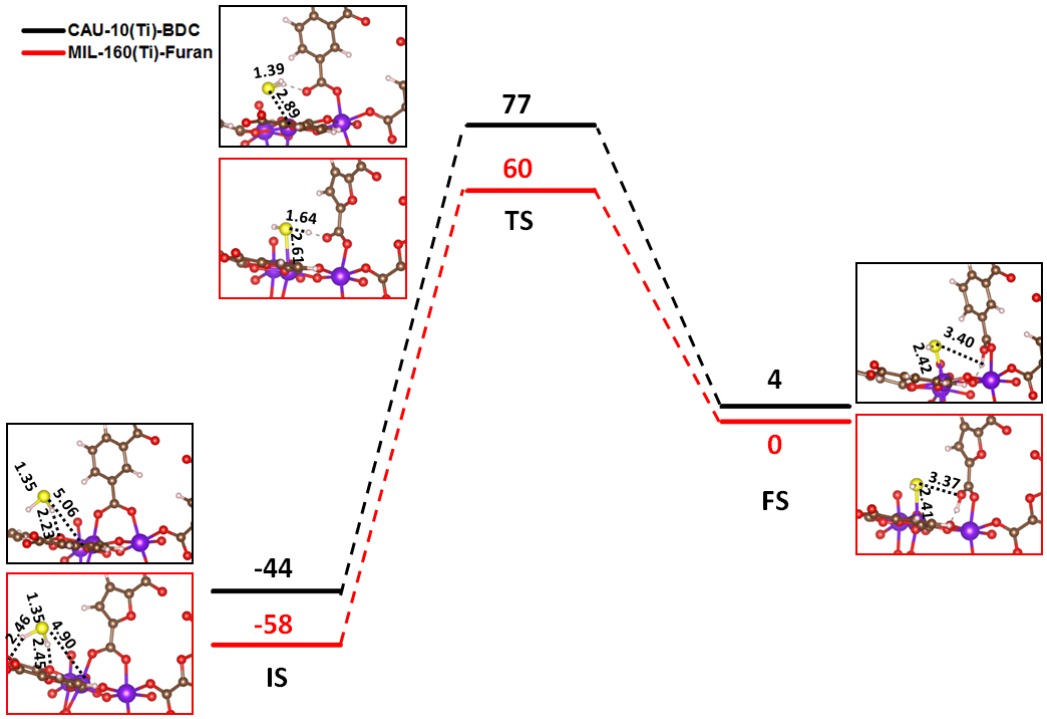

Figure 6: Potential energy profiles for first-step H_2S degradation reaction by CAU-10(Ti)-BDC (black line) and MIL-160(Ti)-Furan (red line). Color code is the same as in Figure 1 except titanium (purple). The corresponding energies and distances are reported in kJ mol^{-1} and Å respectively.

3.6 Impact of the presence and nature of CUS sites on the H_2S stability of MOFs

The influence of the presence and nature of CUS sites on the H_2S stability of the MOF architecture was typcally explored with the consideration of the well-known MOF-74

architecture in its Ni [57] and Zn [52] versions. Figure 7 shows that the most stable adsorption configuration of H_2S in MOF-74(Ni), corresponds to a S-end coordination towards the metal site (IS). The reaction further proceeds as follows: one of the Ni-O bonds breaks, the resulting 3-coordinated O atom forms an oxo μ-O species and one of the H atoms from H_2S transfers to the μ-O to form a μ-OH (FS). Ni becomes 5-coordinated in FS, in comparison to its 6-coordinated geometry in IS. The rate constant associated with this MOF is simulated to be more negative ($-5.\times10^{-6}$) than our reference MIL-53(Al)-BDC (-4.9×10^{-9}). Indeed MOF-74(Ni) is predicted to be stable upon exposure to H_2S which is in excellent agreement with the experimental observation.[57]

Next we considered MOF-74(Zn). The H_2S adsorption geometry (IS) is similar to that observed for MOF-74(Ni) while associated with a slightly lower energy (see Figure 7), however the reaction proceeds in a slightly different manner. We can observe that TS shows one of the μ-O atom unsaturated due to the Zn-O bond breaking, while one of the H atom from H_2S transfers to the unsaturated oxygen atom to form a OH group; next the H atom further transfers to a μ-O formed by a breaking of a second Zn-O bond, and the dangling oxygen atom bonds to Zn again to form the FS. The energy barrier and reaction energy are significantly lower than the values obtained for MOF-74(Ni), indicating that this reaction is more feasible than that involved in MOF-74(Zn). The resulting rate constant for MOF-74(Zn) (-2.0×10^{-11}) is much less negative than MOF-74 (Ni) and our reference MIL-53(Al)-BDC. Therefore MOF-74(Zn) is predicted to be much less stable compared to its Ni analogue. This simulated trend is in excellent agreement with previous experimental observations which revealed MOF-74(Zn) unstable upon H_2S adsorption.[52, 57] This computational work confirms that the H_2S stability of CUS-containing MOFs can be tuned by adopting the adequate nature of metal sites.

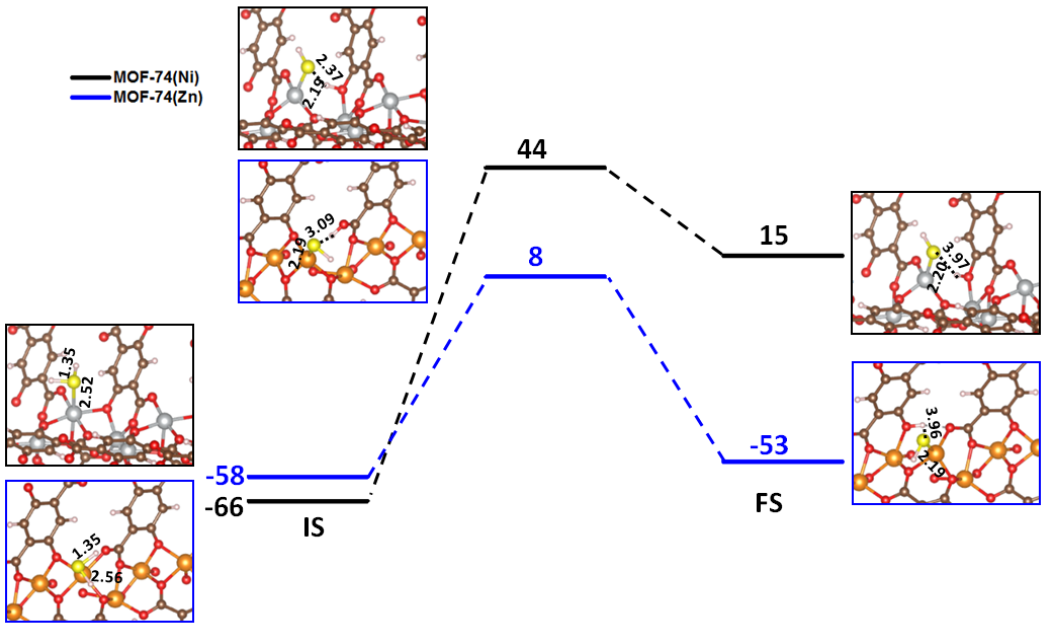

Figure 7: Potential energy profiles for first-step H_2S degradation reaction by MOF-74(Ni) (black line), and MOF-74(Zn) (blue line). Color code is the same as in Figure 1 except nickel (silver) and zinc (orange). The corresponding energies and distances are reported in kJ mol^{-1} and Å respectively.

4. Discussion

Based on the rate constants of the first-step H_2S degradation reaction reported in Table 1, the series of MOFs can be classified in terms of H_2S stability as follows:

CAU-10(Ti)-BDC ~ CAU-10(Al)-BDC ~ MOF-74(Zn) < MIL-53(Al)-FA ~ MIL-160(Ti)-Furan ~ MIL-53(Al)-BDC ~ MIL-160(Al)-Furan ~ lp-MIL-53(Al)-BDC-NO_2 ~ lp-MIL-53(Al)-BDC-NH_2 < np-MIL-53(Al)-BDC-NH_2 < MOF-74(Ni) < MIL-53(Al)-TDC

MIL-53(Al)-TDC is found to be the most stable MOF architecture upon exposure to H_2S. From this ranking, MIL-53 MOFs regardless of linkers/functional groups are expected to be rather stable, since MIL-53(Al)-FA, the predicted least stable MIL-53 was already reported to be stable against H_2S.[54] Furthermore, the CAU-10 frameworks are expected to be unstable under

exposure to H_2S since similar rate constant value was found than MOF-74(Zn) which was demonstrated to collapse upon H_2S adsorption. As a further predictive stage, we extended our study to predict the H_2S stability of the MIL-91(Ti) MOF which demonstrated good promises for CO_2 capture.[70] Based on the stability ranking revealed above, since this material does not exhibit CUS sites, shows a high degree of confinement and its linker contains heteroatoms (N and P), it is expected to show good stability against H_2S. MIL-91(Ti) was then investigated with the consideration of the degradation model reaction defined above.

Figure 8 shows that the most stable adsorption configuration of H_2S (IS) is an H-end configuration over the oxygen atom of the phosphonate group of the MOF linker. The reaction proceeds via the breaking of one Ti-O bond and the formation of a Ti-S bond, while an H atom of H_2S transfers to the PO_3^- group to form a PO_3H group (FS). This process is associated with a very high energy barrier which makes it kinetically and thermodynamically unfavorable. The resulting rate constant calculated is found to be highly negative (-8.3×10^{-4}) indicating that MIL-91(Ti) is expected to be highly stable against H_2S.

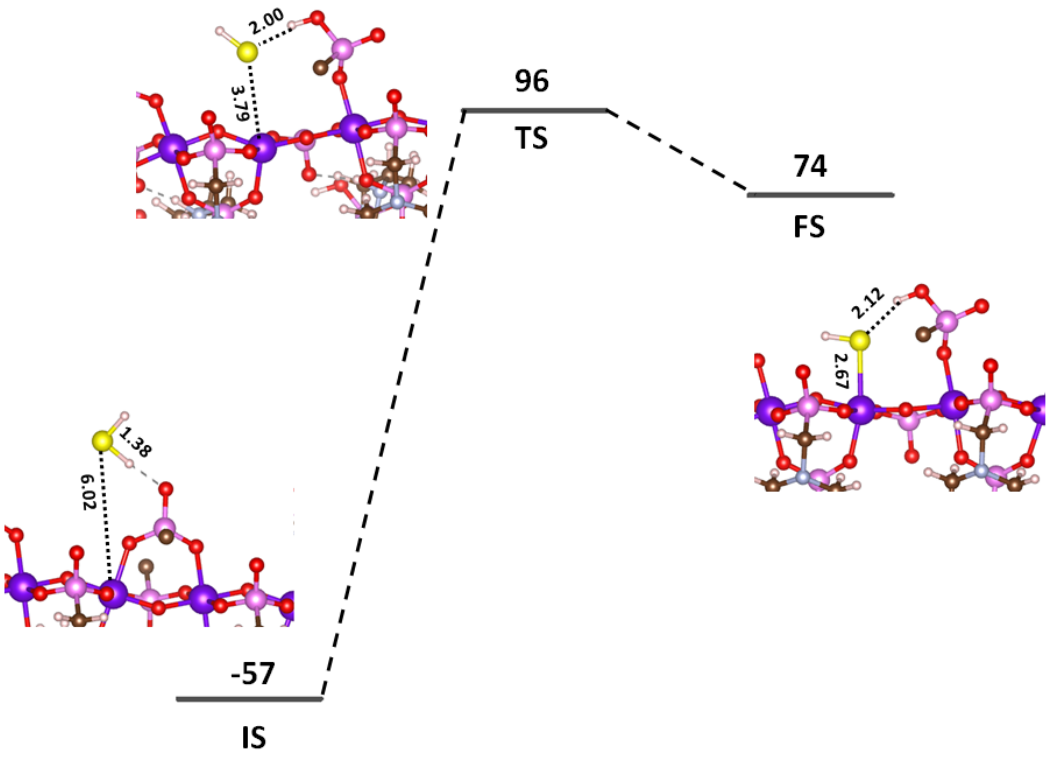

Figure 8: Potential energy profiles for first-step H_2S degradation reaction by MIL-91(Ti). Color code: carbon (brown), oxygen (red), hydrogen (white), sulfur (yellow), nitrogen (blue), phosphorus (pink) and titanium (purple). The corresponding energies and distances are reported in kJ mol^{-1} and Å respectively.

5. Conclusion

In summary, this computational study delivers a systematic assessment of the H_2S stability of a series of MOFs based on the exploration of the first-step degradation reaction. We first analyzed three plausible mechanisms using MIL-53(Al)-BDC as a model MOF and determined the most likely degradation mechanism. The rate constant of the first-step degradation reaction was proposed as a reliable descriptor for characterizing the H_2S stability of MOFs and further used to assess the H_2S stability of a wide range of MOFs to build up a qualitative H_2S stability ranking. Interestingly, this allowed us to reveal that the incorporation of hetero-atoms in the organic linkers of MIL-53 and CAU-10 reinforces their H_2S stability while grafting functional groups or changing the nature of metal sites lead to a similar H_2S stability of the architecture.

MOFs containing CUS sites were also found to show distinct behavior depending on the nature of the metal sites. The MOF MIL-91 (Ti), a promising candidate for CO_2 capture was further considered as a showcase to apply our methodology for the anticipation of its H_2S stability. Our computational approach was demonstrated to allow an accurate and easy handling evaluation of the H_2S stability of MOFs to avoid the use of the highly toxic and corrosive gas in experimental techniques. As a future outlook, we expect to extend our strategy to evaluate the stability of MOFs upon exposure of other corrosive molecules such as SO_x and NH_3. These findings might pave the way towards the identification of key chemical and structural features to guide the development of highly stable MOFs.

ASSOCIATED CONTENT

AUTHOR INFORMATION

Corresponding Author

Guillaume Maurin (guillaume.maurin1@umontpellier.fr)

ORCID: 0000-0002-2096-0450

Pengbo Lyu

ORCID: 0000-0002-1785-9861

Supporting Information

The Supporting Information is available free of charge on the ACS Publications website. It contains all the structural details of MOF systems.

Notes

The authors declare no competing financial interests.

ACKNOWLEDGMENT

This project has received funding from the European Union's Horizon 2020 research and innovation programme under grant agreement N° 837975.

Reference:

(1) Bavykina, A.; Kolobov, N.; Khan, I. S.; Bau, J. A.; Ramirez, A.; Gascon, J. Metal–Organic Frameworks in Heterogeneous Catalysis: Recent Progress, New Trends, and Future Perspectives. *Chem. Rev.* **2020**.
(2) Wang, Q.; Astruc, D. State of the Art and Prospects in Metal–Organic Framework (MOF)-Based and MOF-Derived Nanocatalysis. *Chem. Rev.* **2020,** *120*, 1438-1511.
(3) Wei, Y.-S.; Zhang, M.; Zou, R.; Xu, Q. Metal–Organic Framework-Based Catalysts with Single Metal Sites. *Chem. Rev.* **2020**.
(4) Qian, Q.; Asinger, P. A.; Lee, M. J.; Han, G.; Mizrahi Rodriguez, K.; Lin, S.; Benedetti, F. M.; Wu, A. X.; Chi, W. S.; Smith, Z. P. MOF-Based Membranes for Gas Separations. *Chem. Rev.* **2020,** *120*, 8161-8266.
(5) Liu, X.; Wang, X.; Kapteijn, F. Water and Metal–Organic Frameworks: From Interaction toward Utilization. *Chem. Rev.* **2020,** *120*, 8303-8377.
(6) Adil, K.; Belmabkhout, Y.; Pillai, R. S.; Cadiau, A.; Bhatt, P. M.; Assen, A. H.; Maurin, G.; Eddaoudi, M. Gas/vapour separation using ultra-microporous metal–organic frameworks: insights into the structure/separation relationship. *Chem. Soc. Rev.* **2017,** *46*, 3402-3430.
(7) Maurin, G.; Serre, C.; Cooper, A.; Férey, G. The new age of MOFs and of their porous-related solids. *Chem. Soc. Rev.* **2017,** *46*, 3104-3107.
(8) Horcajada, P.; Gref, R.; Baati, T.; Allan, P. K.; Maurin, G.; Couvreur, P.; Férey, G.; Morris, R. E.; Serre, C. Metal–Organic Frameworks in Biomedicine. *Chem. Rev.* **2012,** *112*, 1232-1268.
(9) Terzopoulou, A.; Nicholas, J. D.; Chen, X.-Z.; Nelson, B. J.; Pané, S.; Puigmartí-Luis, J. Metal–Organic Frameworks in Motion. *Chem. Rev.* **2020**.
(10) Li, C.; Wang, K.; Li, J.; Zhang, Q. Recent Progress in Stimulus-Responsive Two-Dimensional Metal–Organic Frameworks. *ACS Materials Letters* **2020,** *2*, 779-797.
(11) Lim, D.-W.; Kitagawa, H. Proton Transport in Metal–Organic Frameworks. *Chem. Rev.* **2020,** *120*, 8416-8467.
(12) Islamoglu, T.; Chen, Z.; Wasson, M. C.; Buru, C. T.; Kirlikovali, K. O.; Afrin, U.; Mian, M. R.; Farha, O. K. Metal–Organic Frameworks against Toxic Chemicals. *Chem. Rev.* **2020**.
(13) Xie, L. S.; Skorupskii, G.; Dincă, M. Electrically Conductive Metal–Organic Frameworks. *Chem. Rev.* **2020,** *120*, 8536-8580.
(14) Thorarinsdottir, A. E.; Harris, T. D. Metal–Organic Framework Magnets. *Chem. Rev.* **2020,** *120*, 8716-8789.
(15) Ding, M.; Flaig, R. W.; Jiang, H.-L.; Yaghi, O. M. Carbon capture and conversion using metal–organic frameworks and MOF-based materials. *Chem. Soc. Rev.* **2019,** *48*, 2783-2828.
(16) Avci, G.; Erucar, I.; Keskin, S. Do New MOFs Perform Better for CO2 Capture and H2 Purification? Computational Screening of the Updated MOF Database. *ACS Appl. Mater. Inter.* **2020,** *12*, 41567-41579.
(17) Li, Z.; Liu, P.; Ou, C.; Dong, X. Porous Metal–Organic Frameworks for Carbon Dioxide Adsorption and Separation at Low Pressure. *ACS Sustain. Chem. Eng.* **2020,** *8*, 15378-15404.
(18) Liang, W.; Bhatt, P. M.; Shkurenko, A.; Adil, K.; Mouchaham, G.; Aggarwal, H.; Mallick, A.; Jamal, A.; Belmabkhout, Y.; Eddaoudi, M. A Tailor-Made Interpenetrated MOF with Exceptional Carbon-Capture Performance from Flue Gas. *Chem* **2019,** *5*, 950-963.

(19) Liu, J.; Wei, Y.; Zhao, Y. Trace Carbon Dioxide Capture by Metal–Organic Frameworks. *ACS Sustain. Chem. Eng.* **2019,** *7*, 82-93.
(20) Mohideen, M. I. H.; Pillai, R. S.; Adil, K.; Bhatt, P. M.; Belmabkhout, Y.; Shkurenko, A.; Maurin, G.; Eddaoudi, M. A Fine-Tuned MOF for Gas and Vapor Separation: A Multipurpose Adsorbent for Acid Gas Removal, Dehydration, and BTX Sieving. *Chem* **2017,** *3*, 822-833.
(21) Tchalala, M. R.; Bhatt, P. M.; Chappanda, K. N.; Tavares, S. R.; Adil, K.; Belmabkhout, Y.; Shkurenko, A.; Cadiau, A.; Heymans, N.; De Weireld, G.; Maurin, G.; Salama, K. N.; Eddaoudi, M. Fluorinated MOF platform for selective removal and sensing of SO2 from flue gas and air. *Nat. Commun.* **2019,** *10*, 1328.
(22) Wang, H.; Yuan, B.; Hao, R.; Zhao, Y.; Wang, X. A critical review on the method of simultaneous removal of multi-air-pollutant in flue gas. *Chem. Eng. J.* **2019,** *378*, 122155.
(23) Brandt, P.; Nuhnen, A.; Lange, M.; Möllmer, J.; Weingart, O.; Janiak, C. Metal–Organic Frameworks with Potential Application for SO2 Separation and Flue Gas Desulfurization. *ACS Appl. Mater. Inter.* **2019,** *11*, 17350-17358.
(24) Belmabkhout, Y.; Pillai, R. S.; Alezi, D.; Shekhah, O.; Bhatt, P. M.; Chen, Z.; Adil, K.; Vaesen, S.; De Weireld, G.; Pang, M.; Suetin, M.; Cairns, A. J.; Solovyeva, V.; Shkurenko, A.; El Tall, O.; Maurin, G.; Eddaoudi, M. Metal–organic frameworks to satisfy gas upgrading demands: fine-tuning the soc-MOF platform for the operative removal of H2S. *J. Mater. Chem. A* **2017,** *5*, 3293-3303.
(25) Belmabkhout, Y.; Bhatt, P. M.; Adil, K.; Pillai, R. S.; Cadiau, A.; Shkurenko, A.; Maurin, G.; Liu, G.; Koros, W. J.; Eddaoudi, M. Natural gas upgrading using a fluorinated MOF with tuned H2S and CO2 adsorption selectivity. *Nature Energy* **2018,** *3*, 1059-1066.
(26) Yang, Q.; Wiersum, A. D.; Llewellyn, P. L.; Guillerm, V.; Serre, C.; Maurin, G. Functionalizing porous zirconium terephthalate UiO-66(Zr) for natural gas upgrading: a computational exploration. *Chem. Commun.* **2011,** *47*, 9603-9605.
(27) Cheng, Y.; Wang, Z.; Zhao, D. Mixed Matrix Membranes for Natural Gas Upgrading: Current Status and Opportunities. *Ind. Eng. Chem. Res.* **2018,** *57*, 4139-4169.
(28) Silas, K.; Ghani, W. A. W. A. K.; Choong, T. S. Y.; Rashid, U. Carbonaceous materials modified catalysts for simultaneous SO2/NOx removal from flue gas: A review. *Catal. Rev.* **2019,** *61*, 134-161.
(29) Martínez-Ahumada, E.; López-Olvera, A.; Jancik, V.; Sánchez-Bautista, J. E.; González-Zamora, E.; Martis, V.; Williams, D. R.; Ibarra, I. A. MOF Materials for the Capture of Highly Toxic H2S and SO2. *Organometallics* **2020,** *39*, 883-915.
(30) Daglar, H.; Keskin, S. Computational Screening of Metal–Organic Frameworks for Membrane-Based CO2/N2/H2O Separations: Best Materials for Flue Gas Separation. *J. Phys. Chem. C* **2018,** *122*, 17347-17357.
(31) Sumida, K.; Rogow, D. L.; Mason, J. A.; McDonald, T. M.; Bloch, E. D.; Herm, Z. R.; Bae, T.-H.; Long, J. R. Carbon Dioxide Capture in Metal–Organic Frameworks. *Chem. Rev.* **2012,** *112*, 724-781.
(32) Qian, X.; Zhang, R.; Chen, L.; Lei, Y.; Xu, A. Surface Hydrophobic Treatment of Water-Sensitive DUT-4 Metal–Organic Framework To Enhance Water Stability for Hydrogen Storage. *ACS Sustain. Chem. Eng.* **2019,** *7*, 16007-16012.
(33) Xing, X.-S.; Fu, Z.-H.; Zhang, N.-N.; Yu, X.-Q.; Wang, M.-S.; Guo, G.-C. High proton conduction in an excellent water-stable gadolinium metal–organic framework. *Chem. Commun.* **2019,** *55*, 1241-1244.
(34) Lenzen, D.; Eggebrecht, J. G.; Mileo, P. G. M.; Fröhlich, D.; Henninger, S.; Atzori, C.; Bonino, F.; Lieb, A.; Maurin, G.; Stock, N. Unravelling the water adsorption in a robust iron carboxylate metal–organic framework. *Chem. Commun.* **2020,** *56*, 9628-9631.
(35) Karmakar, A.; Mileo, P. G. M.; Bok, I.; Peh, S. B.; Zhang, J.; Yuan, H.; Maurin, G.; Zhao, D. Thermo-Responsive MOF/Polymer Composites for Temperature-Mediated Water Capture and Release. *Angew. Chem. Int. Ed.* **2020,** *59*, 11003-11009.
(36) Xu, L.; Li, Y.; Pan, Q.; Wang, D.; Li, S.; Wang, G.; Chen, Y.; Zhu, P.; Qin, W. Dual-Mode Light-Emitting Lanthanide Metal–Organic Frameworks with High Water and Thermal Stability and Their Application in White LEDs. *ACS Appl. Mater. Inter.* **2020,** *12*, 18934-18943.

(37) Nguyen, H. L.; Hanikel, N.; Lyle, S. J.; Zhu, C.; Proserpio, D. M.; Yaghi, O. M. A Porous Covalent Organic Framework with Voided Square Grid Topology for Atmospheric Water Harvesting. *J. Am. Chem. Soc.* **2020,** *142*, 2218-2221.
(38) Zuluaga, S.; Fuentes-Fernandez, E. M. A.; Tan, K.; Xu, F.; Li, J.; Chabal, Y. J.; Thonhauser, T. Understanding and controlling water stability of MOF-74. *J. Mater. Chem. A* **2016,** *4*, 5176-5183.
(39) Xue, W.; Zhang, Z.; Huang, H.; Zhong, C.; Mei, D. Theoretical Insights into the Initial Hydrolytic Breakdown of HKUST-1. *J. Phys. Chem. C* **2020,** *124*, 1991-2001.
(40) Tan, K.; Zuluaga, S.; Gong, Q.; Canepa, P.; Wang, H.; Li, J.; Chabal, Y. J.; Thonhauser, T. Water Reaction Mechanism in Metal Organic Frameworks with Coordinatively Unsaturated Metal Ions: MOF-74. *Chem. Mater.* **2014,** *26*, 6886-6895.
(41) Zhang, C.; Han, C.; Sholl, D. S.; Schmidt, J. R. Computational Characterization of Defects in Metal–Organic Frameworks: Spontaneous and Water-Induced Point Defects in ZIF-8. *The Journal of Physical Chemistry Letters* **2016,** *7*, 459-464.
(42) Cui, K.; Schmidt, J. R. Enabling Efficient and Accurate Computational Studies of MOF Reactivity via QM/MM and QM/QM Methods. *J. Phys. Chem. C* **2020,** *124*, 10550-10560.
(43) Yuan, S.; Feng, L.; Wang, K.; Pang, J.; Bosch, M.; Lollar, C.; Sun, Y.; Qin, J.; Yang, X.; Zhang, P.; Wang, Q.; Zou, L.; Zhang, Y.; Zhang, L.; Fang, Y.; Li, J.; Zhou, H.-C. Stable Metal–Organic Frameworks: Design, Synthesis, and Applications. *Adv. Mater.* **2018,** *30*, 1704303.
(44) Feng, L.; Wang, K.-Y.; Day, G. S.; Ryder, M. R.; Zhou, H.-C. Destruction of Metal–Organic Frameworks: Positive and Negative Aspects of Stability and Lability. *Chem. Rev.* **2020**.
(45) Flores, J. G.; Zárate-Colín, J. A.; Sánchez-González, E.; Valenzuela, J. R.; Gutiérrez-Alejandre, A.; Ramírez, J.; Jancik, V.; Aguilar-Pliego, J.; Zorrilla, M. C.; Lara-García, H. A.; González-Zamora, E.; Guzmán-González, G.; González, I.; Maurin, G.; Ibarra, I. A. Partially Reversible H2S Adsorption by MFM-300(Sc): Formation of Polysulfides. *ACS Appl. Mater. Inter.* **2020,** *12*, 18885-18892.
(46) Carter, J. H.; Morris, C. G.; Godfrey, H. G. W.; Day, S. J.; Potter, J.; Thompson, S. P.; Tang, C. C.; Yang, S.; Schröder, M. Long-Term Stability of MFM-300(Al) toward Toxic Air Pollutants. *ACS Appl. Mater. Inter.* **2020,** *12*, 42949-42954.
(47) Jiang, H.; Zhou, J.; Wang, C.; Li, Y.; Chen, Y.; Zhang, M. Effect of Cosolvent and Temperature on the Structures and Properties of Cu-MOF-74 in Low-temperature NH3-SCR. *Ind. Eng. Chem. Res.* **2017,** *56*, 3542-3550.
(48) Han, S.; Huang, Y.; Watanabe, T.; Nair, S.; Walton, K. S.; Sholl, D. S.; Carson Meredith, J. MOF stability and gas adsorption as a function of exposure to water, humid air, SO2, and NO2. *Microporous Mesoporous Mater.* **2013,** *173*, 86-91.
(49) Vaesen, S.; Guillerm, V.; Yang, Q.; Wiersum, A. D.; Marszalek, B.; Gil, B.; Vimont, A.; Daturi, M.; Devic, T.; Llewellyn, P. L.; Serre, C.; Maurin, G.; De Weireld, G. A robust amino-functionalized titanium(iv) based MOF for improved separation of acid gases. *Chem. Commun.* **2013,** *49*, 10082-10084.
(50) Hamon, L.; Serre, C.; Devic, T.; Loiseau, T.; Millange, F.; Férey, G.; Weireld, G. D. Comparative Study of Hydrogen Sulfide Adsorption in the MIL-53(Al, Cr, Fe), MIL-47(V), MIL-100(Cr), and MIL-101(Cr) Metal−Organic Frameworks at Room Temperature. *J. Am. Chem. Soc.* **2009,** *131*, 8775-8777.
(51) Hamon, L.; Leclerc, H.; Ghoufi, A.; Oliviero, L.; Travert, A.; Lavalley, J.-C.; Devic, T.; Serre, C.; Férey, G.; De Weireld, G.; Vimont, A.; Maurin, G. Molecular Insight into the Adsorption of H2S in the Flexible MIL-53(Cr) and Rigid MIL-47(V) MOFs: Infrared Spectroscopy Combined to Molecular Simulations. *J. Phys. Chem. C* **2011,** *115*, 2047-2056.
(52) Liu, J.; Wei, Y.; Li, P.; Zhao, Y.; Zou, R. Selective H2S/CO2 Separation by Metal–Organic Frameworks Based on Chemical-Physical Adsorption. *J. Phys. Chem. C* **2017,** *121*, 13249-13255.
(53) Sánchez-González, E.; Mileo, P. G. M.; Sagastuy-Breña, M.; Álvarez, J. R.; Reynolds, J. E.; Villarreal, A.; Gutiérrez-Alejandre, A.; Ramírez, J.; Balmaseda, J.; González-Zamora, E.; Maurin, G.; Humphrey, S. M.; Ibarra, I. A. Highly reversible sorption of H2S and CO2 by an environmentally friendly Mg-based MOF. *J. Mater. Chem. A* **2018,** *6*, 16900-16909.

(54) Shen, J.; Dailly, A.; Beckner, M. Natural gas sorption evaluation on microporous materials. *Microporous Mesoporous Mater.* **2016,** *235*, 170-177.
(55) Zárate, J. A.; Sánchez-González, E.; Jurado-Vázquez, T.; Gutiérrez-Alejandre, A.; González-Zamora, E.; Castillo, I.; Maurin, G.; Ibarra, I. A. Outstanding reversible H2S capture by an Al(iii)-based MOF. *Chem. Commun.* **2019,** *55*, 3049-3052.
(56) Liu, G.; Cadiau, A.; Liu, Y.; Adil, K.; Chernikova, V.; Carja, I.-D.; Belmabkhout, Y.; Karunakaran, M.; Shekhah, O.; Zhang, C.; Itta, A. K.; Yi, S.; Eddaoudi, M.; Koros, W. J. Enabling Fluorinated MOF-Based Membranes for Simultaneous Removal of H2S and CO2 from Natural Gas. *Angew. Chem. Int. Ed.* **2018,** *57*, 14811-14816.
(57) Allan, P. K.; Wheatley, P. S.; Aldous, D.; Mohideen, M. I.; Tang, C.; Hriljac, J. A.; Megson, I. L.; Chapman, K. W.; De Weireld, G.; Vaesen, S.; Morris, R. E. Metal–organic frameworks for the storage and delivery of biologically active hydrogen sulfide. *Dalton Trans.* **2012,** *41*, 4060-4066.
(58) Petit, C.; Mendoza, B.; Bandosz, T. J. Hydrogen Sulfide Adsorption on MOFs and MOF/Graphite Oxide Composites. *ChemPhysChem* **2010,** *11*, 3678-3684.
(59) Zheng, X.-X.; Shen, L.-J.; Chen, X.-P.; Zheng, X.-H.; Au, C.-T.; Jiang, L.-L. Amino-Modified Fe-Terephthalate Metal–Organic Framework as an Efficient Catalyst for the Selective Oxidation of H2S. *Inorg. Chem.* **2018,** *57*, 10081-10089.
(60) Guo, L.; Wang, M.; Cao, D. A Novel Zr-MOF as Fluorescence Turn-On Probe for Real-Time Detecting H2S Gas and Fingerprint Identification. *Small* **2018,** *14*, 1703822.
(61) Zheng, X.-X.; Fang, Z.-P.; Dai, Z.-J.; Cai, J.-M.; Shen, L.-J.; Zhang, Y.-F.; Au, C.-T.; Jiang, L.-L. Iron-Based Metal–Organic Frameworks as Platform for H2S Selective Conversion: Structure-Dependent Desulfurization Activity. *Inorg. Chem.* **2020,** *59*, 4483-4492.
(62) Zhang, X.; Zhang, Q.; Yue, D.; Zhang, J.; Wang, J.; Li, B.; Yang, Y.; Cui, Y.; Qian, G. Flexible Metal–Organic Framework-Based Mixed-Matrix Membranes: A New Platform for H2S Sensors. *Small* **2018,** *14*, 1801563.
(63) Leubner, S.; Stäglich, R.; Franke, J.; Jacobsen, J.; Gosch, J.; Siegel, R.; Reinsch, H.; Maurin, G.; Senker, J.; Yot, P. G.; Stock, N. Solvent Impact on the Properties of Benchmark Metal–Organic Frameworks: Acetonitrile-Based Synthesis of CAU-10, Ce-UiO-66, and Al-MIL-53. *Chem.-Eur. J.* **2020,** *26*, 3877-3883.
(64) Lenzen, D.; Zhao, J.; Ernst, S.-J.; Wahiduzzaman, M.; Ken Inge, A.; Fröhlich, D.; Xu, H.; Bart, H.-J.; Janiak, C.; Henninger, S.; Maurin, G.; Zou, X.; Stock, N. A metal–organic framework for efficient water-based ultra-low-temperature-driven cooling. *Nat. Commun.* **2019,** *10*, 3025.
(65) Wahiduzzaman, M.; Lenzen, D.; Maurin, G.; Stock, N.; Wharmby, M. T. Rietveld Refinement of MIL-160 and Its Structural Flexibility Upon H2O and N2 Adsorption. *Eur. J. Inorg. Chem.* **2018,** *2018*, 3626-3632.
(66) Biswas, S.; Ahnfeldt, T.; Stock, N. New Functionalized Flexible Al-MIL-53-X (X = -Cl, -Br, -CH3, -NO2, -(OH)2) Solids: Syntheses, Characterization, Sorption, and Breathing Behavior. *Inorg. Chem.* **2011,** *50*, 9518-9526.
(67) Stavitski, E.; Pidko, E. A.; Couck, S.; Remy, T.; Hensen, E. J. M.; Weckhuysen, B. M.; Denayer, J.; Gascon, J.; Kapteijn, F. Complexity behind CO2 Capture on NH2-MIL-53(Al). *Langmuir* **2011,** *27*, 3970-3976.
(68) Wang, S.; Cabrero-Antonino, M.; Navalón, S.; Cao, C.-c.; Tissot, A.; Marrot, J.; Martineau-Corcos, C.; Shepard, W.; García, H.; Serre, C. A Robust Titanium Isophthalate Metal-Organic Framework for Visible Light Photocatalytic CO 2 Methanation. **2020**, DOI: 10.2139/ssrn.3570570.
(69) Cadiau, A.; Lee, J. S.; Damasceno Borges, D.; Fabry, P.; Devic, T.; Wharmby, M. T.; Martineau, C.; Foucher, D.; Taulelle, F.; Jun, C.-H.; Hwang, Y. K.; Stock, N.; De Lange, M. F.; Kapteijn, F.; Gascon, J.; Maurin, G.; Chang, J.-S.; Serre, C. Design of Hydrophilic Metal Organic Framework Water Adsorbents for Heat Reallocation. *Adv. Mater.* **2015,** *27*, 4775-4780.
(70) Benoit, V.; Pillai, R. S.; Orsi, A.; Normand, P.; Jobic, H.; Nouar, F.; Billemont, P.; Bloch, E.; Bourrelly, S.; Devic, T.; Wright, P. A.; de Weireld, G.; Serre, C.; Maurin, G.; Llewellyn, P. L. MIL-

91(Ti), a small pore metal–organic framework which fulfils several criteria: an upscaled green synthesis, excellent water stability, high CO2 selectivity and fast CO2 transport. *J. Mater. Chem. A* **2016,** *4*, 1383-1389.
(71) Perdew, J. P.; Burke, K.; Ernzerhof, M. Generalized Gradient Approximation Made Simple. *Phys. Rev. Lett.* **1996,** *77*, 3865-3868.
(72) Blöchl, P. E. Projector augmented-wave method. *Phys. Rev. B* **1994,** *50*, 17953-17979.
(73) Kresse, G.; Furthmüller, J. Efficiency of ab-initio total energy calculations for metals and semiconductors using a plane-wave basis set. *Comp. Mater. Sci.* **1996,** *6*, 15-50.
(74) Kresse, G.; Joubert, D. From ultrasoft pseudopotentials to the projector augmented-wave method. *Phys. Rev. B* **1999,** *59*, 1758-1775.
(75) Grimme, S.; Antony, J.; Ehrlich, S.; Krieg, H. A consistent and accurate ab initio parametrization of density functional dispersion correction (DFT-D) for the 94 elements H-Pu. *J. Chem. Phys.* **2010,** *132*, 154104.
(76) Dudarev, S. L.; Botton, G. A.; Savrasov, S. Y.; Humphreys, C. J.; Sutton, A. P. Electron-energy-loss spectra and the structural stability of nickel oxide: An LSDA+U study. *Phys. Rev. B* **1998,** *57*, 1505-1509.
(77) Wang, L.; Maxisch, T.; Ceder, G. Oxidation energies of transition metal oxides within the GGA+U framework. *Phys. Rev. B* **2006,** *73*, 195107.
(78) Hu, Z.; Metiu, H. Choice of U for DFT+U Calculations for Titanium Oxides. *J. Phys. Chem. C* **2011,** *115*, 5841-5845.
(79) Henkelman, G.; Uberuaga, B. P.; Jónsson, H. A climbing image nudged elastic band method for finding saddle points and minimum energy paths. *J. Chem. Phys.* **2000,** *113*, 9901-9904.
(80) Henkelman, G. "Vasp TST tools". http://theory.cm.utexas.edu/vtsttools/.
(81) Arevalo, R. L.; Escaño, M. C. S.; Kasai, H. Computational Mechanistic Study of Borohydride Electrochemical Oxidation on Au3Ni(111). *J. Phys. Chem. C* **2013,** *117*, 3818-3825.
(82) Mounfield, W. P.; Han, C.; Pang, S. H.; Tumuluri, U.; Jiao, Y.; Bhattacharyya, S.; Dutzer, M. R.; Nair, S.; Wu, Z.; Lively, R. P.; Sholl, D. S.; Walton, K. S. Synergistic Effects of Water and SO2 on Degradation of MIL-125 in the Presence of Acid Gases. *J. Phys. Chem. C* **2016,** *120*, 27230-27240.

TOC: